Non-LTE radiative transfer in clumpy molecular clouds

M. Juvela

Helsinki University Observatory, Tähtitorninmäki, P.O.Box 14, FIN-00014 University of Helsinki, Finland

Abstract. We present some results of the simulation of radiative transfer in clumpy molecular clouds. For this study we have developed a program that can be used to calculate the observed molecular line profiles with one–, two– and three-dimensional model clouds. The three-dimensional models enable us to study the effect of small-scale density fluctuations on the observed molecular emission lines. The density distributions can be generated by using either fractal models or structure tree statistics.

We have made some modifications to the traditional Monte Carlo simulation scheme. These changes can in some cases significantly speed up the simulation and e.g. enable efficient calculations of clouds with high optical depths. We shall describe the principles of the implemented algorithms and present some CS spectra calculated using different clumpy cloud models.

The model calculations have confirmed that clumpy cloud structure combined with macroturbulent motions can decisively reduce self-absorption seen in molecular lines. Such effects indicate that the estimation of e.g. the column density is very uncertain without detailed knowledge of the density structure of the cloud.

Key words: radiative transfer – line: profiles – ISM: clouds – ISM: molecules – radio lines: ISM

1. Introduction

Monte Carlo (MC) simulation is a very flexible method for carrying out radiative transfer calculations. From early on it has been used both for spectral line calculations (e.g. Magnan 1970) and for the simulation of light scattering (e.g. Sandford 1973; Mattila 1970). It was quickly recognized that with MC one is not limited to simple models e.g. the effects of inhomogeneities in the cloud structure could be studied (van Blerkom 1971). However, most of the models remained still relatively simple. In 1979 Bernes published an important article on the use of MC for molecular emission line calculations. The model clouds were spherically symmetric and had a uniform density.

Over the years, as computing power has increased, the models used in MC calculations have become more detailed. MC simulation is a very common tool in studies of light scattering

(e.g. Whitney & Hartmann 1992; Fischer et al. 1994; Lehtinen & Mattila 1996; Voshchinnikov et al. 1996; Fischer et al. 1996). Over the past few years MC has been used extensively also in the study of line emission in e.g. comets (Rousselot et al. 1994), accretion disks (Knigge et al. 1995), masers (Spaans & Langevelde 1992), supernovae (Mazzali & Lucy 1993; Mazzali et al. 1995; Zhang & Wang 1996) and molecular clouds (e.g. Gonzáles-Alfonso & Cernicharo 1993; Choi et al. 1995).

CS observations of interstellar clouds have been modeled lately with MC calculations by Zinchenko et al. (1994) and Choi et al. (1995). In these studies the model clouds have been spherically symmetric i.e. essentially one-dimensional. Molecular clouds have, however, a much more complicated structure and the interest in the study of these inhomogeneities has increased. The effects of inhomogeneity on the temperature structure and chemistry of interstellar molecular clouds have already been studied by Boisse (1990) and Spaans (1996) with the aid of MC simulations.

In order to study the effects of small scale density fluctuations on molecular emission lines, the Monte Carlo procedure has been extended to full three-dimensional cloud models (Park & Hong 1995, 1996). The advances in computer technology have made it possible to study more realistic models. In the future further computer development is likely to increase the importance of the Monte Carlo method.

Monte Carlo calculations of the radiative transfer problem are based on the simulation of the basic physical processes with the aid of computer-generated random numbers. Compared with other methods of solution MC simulation is extremely simple since one has to deal only with the basic formulae of the simulated physical processes.

Besides simplicity MC has also other significant advantages in radiative transfer calculations. MC simulation does not require simplifying assumptions as in micro-turbulent (e.g. Leung & Liszt 1976; Liszt & Leung 1977) or large velocity gradient (LVG) models (e.g. Goldreich & Kwan 1974; de Jong et al. 1975). The velocity field as well as the the density distribution of the cloud can be arbitrary. Therefore clumpy clouds can be studied with essentially the same program as simple, spherically symmetric clouds.

The long CPU–time needed for the simulation is almost the only negative side of the MC method. The random error in

the results is approximately inversely proportional to the square root of the number of simulated photons and therefore a substantially increased accuracy can be obtained only at the cost of much longer computing times. The situation gets worse with higher dimensions. If a cloud is discretized in three dimensions each simulated photon interacts only with a small fraction of all the cells. The dependence between the number of cells and the required execution time is over-linear. For these reasons one is forced to use a low resolution discretization for the studied cloud.

A reference field was used by Bernes (1979) as a way to reduce the errors associated with the use of random numbers. In addition to this method we have also made some other changes and additions to the original simulation scheme and have found that they may, in some cases, reduce the execution times significantly.

The aim of the present study is two-fold. In the first part the methods of radiative transfer simulation are studied. We introduce a new simulation scheme that should prove effective especially in the study of clumpy clouds. We will also discuss some implementation details which can be used to reduce the execution times needed for the simulation.

These principles are embodied into a program that serves as the basis for the second part of this study in which the effects of clumpy density distribution on the observed CS lines are studied. We are mainly interested in qualitative effects, e.g. the existence or absence of the self-absorption features, line broadening etc. Similar studies have already been conducted using the CO molecule (Park & Hong 1995). It is necessary, however, to extend this work to other molecular species and especially those probing higher densities. CS is particularly suitable for this study because it has many easily observable rotational transitions in the mm and sub-mm range.

The density structures of the model clouds will be generated either with structure trees or with fractal models. These distributions are clearly more realistic than what has been used in model calculations so far. The comparison of different density distributions is needed so that the general characteristics of the clumpy cloud structure can be identified. Our knowledge about the exact nature of the small scale clumpiness is still very limited. Comparison of different clumpy models should prove useful in resolving these uncertainties.

This study serves also as a preparation for a more detailed analysis of the CS and $C^{34}S$ observations from southern massive star forming cores (Juvela 1996). In this future work the observations will be interpreted with the aid of model calculations and the correspondence between different cloud models and the observations will be addressed.

After a short presentation of the model clouds in Sect. 2 we shall discuss the implementation of the simulation procedures in Sect. 3. A few test problems as well as some comparisons with earlier simulation programs will be shown in Sect. 4. The results from the molecular line calculations made with clumpy cloud models are shown in Sect. 5 and the results are discussed in Sect. 6. The final conclusions are presented in Sect 7.

2. The model clouds

We have made calculations with clouds of three different geometries. The simplest are spherically symmetric and therefore essentially one-dimensional. The second type is cylindrically symmetric (i.e. two-dimensional) and the third, three-dimensional. In this paper we shall concentrate on the three-dimensional models with some results on the one-dimensional clouds shown for comparison.

For the radiative transfer calculations one must first set the density, velocity field, turbulence and kinetic temperature in each cell of the cloud. These quantities remain unchanged during the calculation and only the relative populations of the different energy levels are changed.

We have used two methods to generate the density distributions of the three-dimensional clouds. These are based on the structure-tree statistics of Houlahan & Scalo (1992) and the fractal model of Hetem Jr. & Lépine (1993). Both methods are based on the the observed properties of the molecular clouds and are not directly linked to theoretical hydrodynamic models.

Structure-tree statistics describes the cloud as a hierarchical structure of clumps. The making of the model cloud starts with one big clump and proceeds recursively as η sub-clumps are generated within each clump. The density distribution of a clump is identical to that of the parent with the size scaled down with some factor, k_L, and the centre density multiplied with another factor, k_n. In our models the clumps have a density distribution $(r/R)^\alpha$, where r is the distance from the centre of the clump, R the size of the structure and α a free parameter.

It is well known that molecular clouds show similar structure on many different scales (see e.g. Dickman et al. 1990; Falgarone et al. 1991). This fractal nature of the clouds seems to extend down to the smallest observable scales, i.e. at least down to 0.01 pc. The fractal dimension of most interstellar clouds is close to 1.3 (see e.g. Dickman et.al. 1990).

We calculate the density of fractal model clouds according to the Model 1 of Hetem & Lépine (1993). The algorithm has only one free parameter, α, which determines the fractal dimension of the cloud. The algorithm starts by dividing a cubic cloud into eight sub-cubes with the mass of the cloud divided between the sub-cubes according to random numbers. The procedure is repeated recursively on all sub-cubes. In order to force the density to increase towards the centre of the cloud we have used the variation in which after each division the densest sub-cell is moved closest to the centre and the least dense cell furthest away (see Hetem & Lépine 1993).

The turbulence in the model clouds is divided into two parts. Microturbulence is the velocity dispersion within a cell and together with the kinetic temperature of the gas it determines the intrinsic line width. Macroturbulence is the random velocity component assigned to a cell. The assignment of turbulence to the model clouds is discussed in more detail in Sect. 5.

3. Principles of the simulation process

In this section we give a general description of the implemented simulation methods. A more detailed description is presented in Appendix 7. We shall concentrate on the calculations performed using three-dimensional cloud models. The same principles also apply to clouds of one or two dimensions.

3.1. The basic simulation methods

We have used two basic methods in the calculations. The first of these (method A) is similar to the traditional Monte Carlo simulation as described by Bernes (1979). The radiation field is simulated with the aid of photon packages which are generated in random locations in the cloud. The cloud itself is divided into a number of cells in which physical parameters are assumed to be constant. Initially the photon package contains a number of photons which is calculated based on the local gas properties and the number of model photons used in the simulation. To improve the efficiency the package contains photons from all simulated transitions. The package is moved in some random direction until it exits the cloud. Every time the package goes through a cell the number of absorbed photons is subtracted from the photon package and added to counters in the cell. The cell contains a separate counter for each transition. Between simulation steps the equilibrium equations are solved in the cells with the aid of the updated counters and the simulation continues with the new population numbers.

The second method (method B) differs from the standard MC method in some important details. Instead of generating emission events in random locations, the model photons are always started at the outer boundary of the cloud. Initially the package contains only background photons and as it goes through a cell the number of absorption events are added to counters in the cells as usual. However, as the package passes through a cell a part of the photons emitted by the cell during one iteration are also added to the photon package. The package goes through a cell with just one step and since this addition is done only at the borders of the cells the photons absorbed within the emitting cell must be dealt with explicitly. Furthermore, since only some of the photons emitted from the cell are added to each passing package the total number of passing photon packages must be known. For this purpose we keep track of the total length that photon packages travel within each cell during one simulation step. On later iterations this knowledge can be used in dividing the total number of emitted photons between the photon packages that go through the cell. In principle the number of passing model photons should be the same for all cells. However, if we repeat the simulation always with the same random numbers we can eliminate the errors caused by the fact that all cells are not always hit by quite the same number of model photons.

Method B has some advantages over method A. First of all, the method guarantees that the photon package will never become empty. However, since photons are added to the package only at the boundaries between the cells, the number of photons

emitted and absorbed within the same cell must be calculated explicitly. In normal Monte Carlo simulation there is no need for this (nor is it possible) since the emission events are generated at random locations and the absorption events in the emitting cell are treated in the same way as in any other cell. This means, however, that in the normal MC method the model photons must be created in many different locations within the cell in order to get the right number of photons out of a cell. If the cell is optically thick only photons emitted on the surface of the cell would be likely to escape. Method B does not present such problems. The number of escaping photons is calculated explicitly, and to achieve the same accuracy using the normal MC method one should generate a large number of emission events along the path of the model photon and literally calculate the integral of escaping photons using Monte Carlo integration. Clearly, doing this integration explicitly is a great advantage if some cells are optically thick. In clumpy clouds the density differences may be large between the cells and method B should be more efficient.

3.2. The use of random numbers

The random numbers used in the simulation process induce random errors into the calculated quantities. This random noise acts as an important indicator of the quality of the results. However, the random component makes it difficult to accurately track the convergence of the population levels.

We have used both a normal pseudorandom number generator, `mzran` (Marsaglia & Zaman 1994), and a quasirandom number generator, `sobseq` (Press & Teukolsky 1989). Pseudorandom numbers simulate true random numbers while the quasirandom numbers are distributed more evenly and are in fact generated to avoid each other. In a real cloud the photons are emitted from truly random locations and towards random directions. During the simulation this large number of real photons must be approximated with a much smaller number of simulated photons and therefore the random fluctuations in the simulated radiation field tend to be much larger. The use of quasirandom numbers should be helpful in this respect since it ensures a more uniform distribution for the generated model photons.

During normal Monte Carlo simulation the number of simulated photon packages going through a cell depends on the location of the cell. In method B, on the other hand, as the packages are always started at the edge of the cloud the density of the paths is approximately constant. It is essential that the number of passing photon packages is the same for all cells, since in method B this affects also the number of photons emitted from the cell. For that reason we favour the use of quasirandom numbers.

The random number generator can be reset after each iteration if the real radiation field is accurately sampled with the model photons generated during one iteration step. In that case the photon package will be sent from the same locations and to the same directions as on the previous iterations and we know the exact number of photon packages passing each cell and the exact amount of photons to be added to each package passing

through a cell. The random fluctuations can be thus eliminated (see Sec. 3.1), the changes in level populations during the iterations will be smooth and the convergence can be followed with great precision.

3.3. Some efficiency issues

The physical conditions within the cells are assumed to be constant and therefore a photon package can always be moved through a cell with just one step. Since the step length is the same irrespective of the photon frequency there is no reason why all transitions should not be treated simultaneously. For this reason a photon package usually contains photons from different transitions.

This approach can be taken one step further. Instead of calculating a single Doppler shift for the emitted model photon we treat the whole line profile at the same time i.e. each photon package contains for each transition an array that gives the number of photons as the function of frequency. This is also needed in order to be able to add photons from different cells to a single photon package when the simulation method B is used. This approach is very efficient since less separate photon packages need to be generated and some common intermediate results can be used to update all channels.

The number of channels must be sufficiently large so that the interactions between cells with different velocities can be calculated with the required accuracy. The cost of calculating N channels is, of course, only N times the cost of calculating one channel or even less if one considers that some calculations are common to all channels. In order to get a comparable accuracy by using model photons with random Doppler shifts, as in the traditional MC method, the required number of model photons far exceeds N and the decrease in random errors is proportional only to $1/\sqrt{N}$.

We have found that using method B almost all of the CPU time is used in updating the photon packages i.e. calculating the number of absorption and emission events in the cells. The time used to calculate the photon path or even the time spent solving the equilibrium equations is insignificant in comparison. In order to avoid calculating the emission and absorption profiles each time a photon package passes a cell, we create at the beginning a two-dimensional array containing Gaussians with different widths. During the simulation emission and absorption profiles are read from this array. A pointer is used to point to the gaussian with the right width and Doppler shifts are taken into account by moving the pointer by the correct number of channels.

In one– and two–dimensional clouds the cells are of different size and e.g. the probability of a package going through the smallest inner spheres in a 1D cloud is very small. Therefore it may be necessary to implement a weighting scheme so that the generated packages are preferentially directed towards the inner parts of the cloud. The weighting is easy to implement in a normal MC-simulation but is even more simple when method B is used. All calculations on 1D models in this paper have been made using such weighting.

3.4. Convergence acceleration

The calculations are usually started with LTE conditions. The number of iterations required to reach an equilibrium state with a given accuracy depends on various properties of the cloud and the molecule, e.g. the number of populated excitation levels. The convergence can be very slow especially if the optical depth of the cloud is very high. This problem is well known and several acceleration methods have been developed for methods other than Monte Carlo simulation (see e.g. Rybicki & Hummer 1991; Dickel & Auer 1994).

If the random fluctuations of the level populations are eliminated by resetting the random number generators after each iteration, the change of the level populations will be smooth. This provides a mean to speed up the calculations of a Monte Carlo simulation.

We have used the following simple scheme. On each iteration the changes in the level populations are computed in the usual manner. In each cell and for each energy level the computed change is first multiplied by a weight w before it is added to the values from the previous iteration. Initially the weights are set to $w=1.0$ which corresponds to the normal updating. However, the weights themselves are also changed during the calculations. Each time the change in the level population has the same sign as on the previous iteration the corresponding weight is multiplied by a factor $1.0 + k$ where $k > 0.0$. On the other hand, if the sign changes the weight is again set to $w=1.0$. This method prevents the program from taking numerous small steps while the current solution is still far from the correct one and the corrections are weighted as long as the computed change is to the same direction as on the previous iterations. As the solution converges it is also necessary to decrease the value of k in order to prevent the level populations from oscillating around the correct value. This can be done by multiplying k on each iteration with some constant $w_k < 1.0$. With correct parameter values this method brings the solution quickly close to the correct one while during the final iterations it has no effect on the calculations. Note that direct extrapolation of the level populations would give very little savings in execution times.

As an example we take the cloud model of Bernes (1979). For calculations the one-dimensional model cloud is divided into 30 spheres of equal volume. In Fig. 1a we show the change in level populations with and without this acceleration method. The iterations were stopped after the relative change of all level populations in all of the 30 spheres was less that 0.005 on one iteration step. With suitable weighting factors the number of required iterations could be brought down by half. At least in this case the solution obtained using the acceleration method seems also to be closer to the correct solution and e.g. the level population of the level J=2 is after 20 iterations the same as it would be after about 50 iterations without acceleration.

In some other clouds we have been able to bring the number of required iterations even down to a third. The best values for the parameters change somewhat from cloud to cloud, but acceleration can normally be achieved within a wide parameter range. Therefore, we think that the method is also of practical

use when studying optically thick clouds. On the other hand, clouds like those in the article by Liszt & Leung (1977) usually require only about ten or less iterations if the same convergence criterion is used. The use of this method may in such cases even increase the number of iterations with one or two.

From Fig. 1a one can also see that testing only the relative changes in the level populations is not always a sufficient or a good convergence criterion. Even though the change per iteration is small the solution might still be far from the correct one. In this case the random number generators were reset after each iteration which means that there is no random noise in the level populations. If this were not so it would be very difficult to devise a meaningful convergence criterion based only on the level populations.

4. Test cases

We have implemented the methods described in the previous sections into a program where we can choose between methods A and B. We can also use the reference field to suppress random noise and choose between two random number generators i.e. use either pseudorandom or quasirandom numbers.

The program has been tested by comparing its results to some model calculations published in the past. We present here the results from the comparison with the microturbulent models of Liszt & Leung (1977). The model cloud of Liszt & Leung has a radius of 2.5 pc, a constant kinetic temperature of 40 K, and an intrinsic linewidth of 3.0 km s^{-1}. The hydrogen density and the fractional abundance of CS are varied so that the column density of CS stays constant (see Fig. 2a in their article). In the calculations we used a value of μ=1.95 D for the permanent dipole moment of the CS molecule and the collision rate constants published by Green and Chapman (1978). These are presumably the same constants as used by Liszt & Leung for collisions between CS and H$_2$. The collisions between CS and He are neglected.

We made the calculations using both the one-dimensional and the full three-dimensional models. The one-dimensional spherical model cloud consisted of 30 shells. The radii of the shells were selected so that all the spherical cells had the same volume. The three-dimensional model cloud consisted of 31×31×31 cells from which the corners were rounded off. Since the radius of the cloud is only some 15 cells, the discretization of the three-dimensional cloud is more coarse. The line profiles calculated with the three-dimensional model cloud were almost identical and the differences could hardly be seen by eye.

We also repeated the calculations with and without the aid of the reference field (using only positive reference temperatures although some transitions may have negative excitation temperatures) and also using traditional Monte Carlo simulation (method A) and our new simulation method (method B). The results remain the same irrespective of the method of calculation. The profiles were compared with the results of Liszt & Leung and the differences in the peak temperatures were less than 0.2 K for all transitions and usually much smaller.

The number of photon packages used in the calculation of the one-dimensional models was also varied. When method B was used and the random number generators were reset on each iteration the changes in the calculated spectra were observable only when the number of photon packages was ∼70 per one iteration. This illustrates the very low number of separate model photons needed with method B. In three-dimensional models 10000 photons per iteration were enough to get results similar to those of the one-dimensional model. Lower photon numbers were not tested.

We reproduced also the results of Park & Hong (1995) for three-dimensional, clumpy clouds with a volume filling factor f=0.12 (Fig. 5 in their article). Using simulation method B we made 15 iterations with 10 000 model photon packages per iteration. This means that on each iteration there are approximately 10 photon packages going through each cell and each package represents the total radiation field in one direction. The spectra were calculated by using a convolving gaussian beam with a FWHM corresponding to four cells. Since the number of cells within the beam is very large, the random errors in the calculated excitation temperatures of individual cells do not show up in the line profiles. All line intensities agree within ∼2% with the results of Park & Hong (1995), and the differences become smaller if more than 15 iterations are made.

In Fig. 1b we show the radial excitation temperature distributions of two ^{12}CO transitions in a cloud with f=1.0. The cloud is similar to the one in Fig. 1 of Park & Hong (1995). The calculations were made using the method B with the aid of a reference field. We used 20 000 model photons per iteration and the figure presents the situation after 15 iterations. In spite of the relatively low number of model photons the result is still quite comparable with the results of Park & Hong (1995).

These results can also be compared with the calculations made by Bernes (1979) using a spherically symmetric model cloud. Although our three-dimensional cloud has a somewhat lower kinetic temperature and no infall velocity the models are still rather similar. For the calculation of the one-dimensional model Bernes (1979) used 200 model photons per iteration and the absorption event counters contained in the end the average over 20 iterations. Our photon numbers cannot be compared directly with this, however, since each of our model photons contains information of the whole line profile and is therefore more expensive to calculate. Even if this is taken into account it seems that the cost of modelling three-dimensional clouds with method B is not excessively high compared with the cost of modelling one-dimensional clouds. We calculated the absorption counters on each step as the average of the values collected during the current iteration and the average from past iterations weighted with 2.0. Increasing this weight (to e.g. 4.0) would considerably lower the noise in the excitation temperatures but would also slow down the convergence. Another possibility would be to use a larger weight to decrease the noise and reset the counters after some iterations to enhance the convergence. In the case of Fig. 1b the line was divided into 30 velocity channels and the calculations took 35 minutes on a Pentium-166MHz computer. Using only 10000 model photons per iteration would
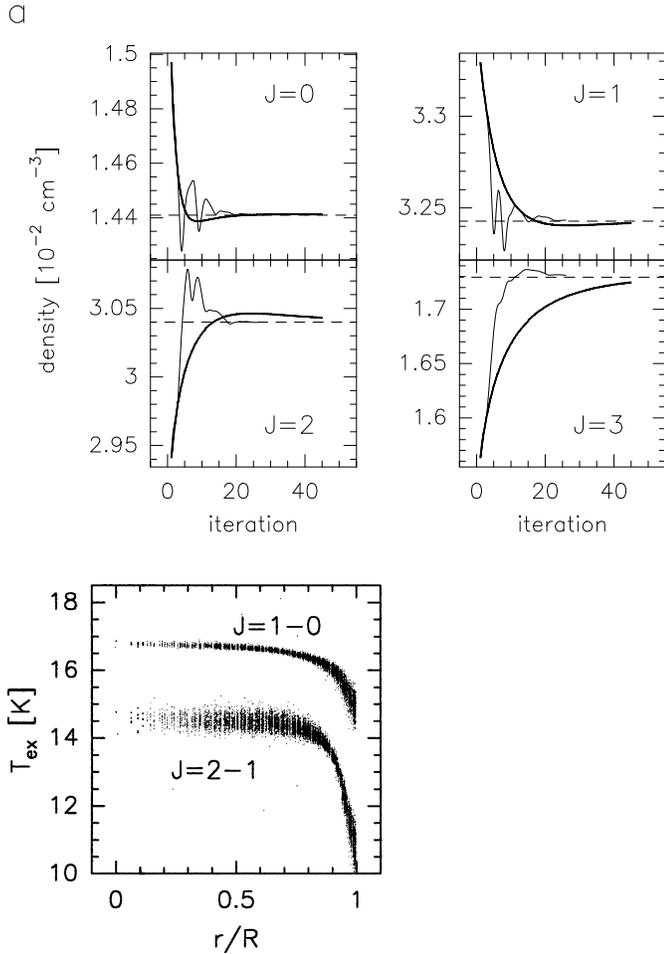
a

Fig. 1. a The change in the level populations of the ^{12}CO molecule in the innermost sphere of a spherically symmetric, one-dimensional cloud. The cloud is identical to the model cloud of Bernes (1979) but divided into 30 spheres of equal volume. The thick lines show the convergence during normal iterations and the thin lines the convergence using our simple acceleration method. The dashed lines indicate the correct values for the level populations. **b** The excitation temperatures of individual cells as the function of distance from the cloud centre in a three-dimensional model cloud similar to the cloud in Fig 1 of Park & Hong (1995). The cloud consists of $31\times31\times31$ cells and has a constant density of $n=2.0\cdot10^3$cm^{-3} and a kinetic temperature of 15 K. The excitation temperatures of the transitions ^{12}CO(1–0) and ^{12}CO(2–1) are shown. The points for the transition J=1–0 have been moved up by 2.0 K. The number of iterations was 15 and the number of photon packages 20 000 per iteration

give higher noise in the excitation temperatures but the computed line profiles would remain much the same.

5. Clumpy clouds

Using the models described in Sect. 2 it is possible to create a large variety of clumpy model clouds for the radiative transfer simulations. In this section we shall present some results of the calculations made with clouds created either with the structure tree model or with the fractal model.

The model clouds consist of $36\times36\times36$ cubic cells. All radiative transfer computations were made using the simulation method B and the number of rotational levels included into the calculations was 11. The lines were divided into 0.25 km s^{-1} wide channels both during the simulation and when calculating the spectrum. The spectra were calculated by convolving the emitted intensity with a gaussian beam. The FWHM of this beam was 6 times the length of the side of an individual cell. In the following the terms cloud diameter and cloud radius will refer to the cloud size along the edge of the cubic cloud.

5.1. Fractal clouds

The method used to create the fractal model clouds (see Sect. 2) has only one parameter, α. The fractal dimension determined from the column density maps was found to depend only weakly on this. The density distribution is more affected with the proportion of denser cells increasing with larger parameter values. It should be noted that the shape of the density spectrum is completely unrelated to the fractal dimension. The fractal dimension is usually determined from the slope of the (log(A),log(P))– relation i.e. from the relation between areas and perimeters of the structures seen in the column density map at different column density levels. The relation is approximately linear and any monotonic transformation of the cell densities will preserve the fractal dimension. Also, for the observed line profiles the mass spectrum is probably much more important.

We present here calculations performed with three fractal clouds, F1, F2 and F3. The clouds have been created using different values of the parameter α: $\alpha=0.1$ for F3, $\alpha=0.4$ for F1 and $\alpha=0.7$ for F2. All clouds have fractal dimensions of about 1.3 and are in this respect similar to real clouds. The fractal dimension was determined from the (log(A),log(P))– relation, but since the column density maps are relatively small, 36×36 pixels, the value of the dimension is consequently somewhat uncertain. We feel, however, that here the fractal dimension is not very important by itself.

The mass spectra of the three clouds are shown in Fig. 2a. In Fig. 2b the column density map of the cloud F1 is shown as an example. During each run the densities of the cloud cells were scaled to desired density ranges with a linear transformation. This scaling does not change the shape of the mass spectrum nor the fractal dimension.

5.1.1. Clouds with macroturbulence

In the model clouds the turbulence consists of two components: the turbulence within the cells and the random motions of the cells themselves. The first of these is reflected only in the intrinsic linewidths which were taken to be the same in all cells. This microturbulent velocity dispersion was set to $\sigma=0.2$ km/s. The macroturbulence was created by assigning to each cell a random velocity component generated from a normal distribution with $\sigma=1.2$ km/s. The linewidth is therefore mainly due to these
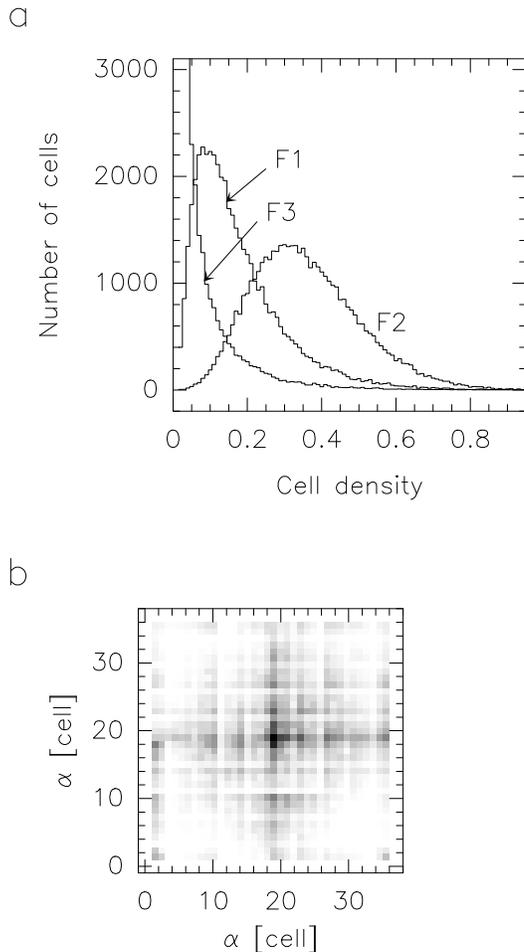
Fig. 2. a The mass spectra of the fractal model clouds F1, F2 and F3. The cell mass is proportional to the cell density which is plotted on the x-axis. **b** The column density map of cloud F1 as seen towards one of the faces of the cubic cloud. This is also the approximate direction towards which the spectra were calculated. The column density scale is arbitrary since the density values were always scaled prior to calculation

cell velocities with smaller contributions from the microturbulence and the thermal line broadening. A small infall velocity $v(r)=v_0\,r^{-\alpha}$ was also added to the clouds with α=0.5 and the velocity at the cloud surface v_0=0.15 km s^{-1}. The results will therefore also indicate under what conditions such a velocity field can be deduced from the observed line profiles.

The results from the initial runs using these model clouds are shown in Fig. 3. The kinetic temperature of the clouds was set to a constant value of T_{kin}=40 K and the calculations were performed with the maximum densities scaled to $1.0\cdot10^5$ cm^{-3}, $5.0\cdot10^5$ cm^{-3} and $1.0\cdot10^6$ cm^{-3}. The cloud size was 0.23 pc×0.23 pc, which would correspond to 48″×48″ if the cloud was at the distance of 1000 pc. The spectra at the central positions of the clouds as well as at distance of 1/3 and 2/3 times the cloud radius are shown.

The differences between the model clouds are mainly due to different column densities which in turn result from the differ-

ences in the mass spectra. Using a beam with FWHM twice the value used in calculating the spectra the beam averaged column densities were $8.04\cdot10^{13}$, $1.51\cdot10^{14}$, and $3.06\cdot10^{13}$ at the centre positions of F1, F2, and F3, respectively when the maximum densities were scaled to $1.0\cdot10^5$ cm^{-3}. The differences between the models can be seen also by comparing the optical depths. The optical depths in the line centre are listed in Table 1.

Cloud F3 has the lowest column densities and no self-absorption can be seen in in its spectra. In clouds F1 and F2 some line profiles are flat-topped due to self-absorption. The effect is strongest for the transitions 3–2 and 5–4 which, in F2, are clearly self-absorbed when the maximum density is $5.0\cdot10^5$ cm^{-3}. At higher densities these lines have clearly non-Gaussian profiles also in F1. Because of the large macroturbulence the line profiles are not very smooth and it is difficult to deduce the existence of the infall motion from the small asymmetry in the lines. The line ratios, for a given model and maximum density, remain nearly constant in all positions.

In Fig. 4 we show the centre point spectra with the kinetic temperature of the clouds set to 20 K. As expected the relative intensity of the transitions CS(2–1) and CS(3–2) has increased. These lines show also stronger self-absorption features at this lower temperature. The change in the kinetic temperature has, however, somewhat different effects in the three model clouds. The line intensities are least affected by the drop in the kinetic temperature in the cloud F3 which has the lowest average density. As the mean density of the model increases the changes in the spectra get more noticeable. Apparently the cloud F3 is optically thin to such an extent that the excitation temperatures are not strongly affected by the kinetic temperature while e.g. cloud F2 is close to thermalization due to its higher average density. While the drop in temperature has generally decreased the intensity of the transitions 5–4 and 7–6, the line CS(5–4) is still flat topped in both high density models, F1 and F2.

It is difficult to say to what extent the differences in the observed spectra are due to the different density distributions in the clouds and to what extent to the different column densities. To study this question we scaled the physical sizes of clouds F1 and F3 in such a way that the column densities at the centre positions of the clouds (averaged over a beam with FWHM twice that used for spectrum calculations) were approximately the same as for F2 in Fig. 3b when the maximum density was scaled to $5.0\cdot10^5$ cm^{-3}. The linear size of F1 was therefore increased by a factor of 1.8 and the size of F3 by a factor of 4.7. Since the beam size is much smaller than the size of the clouds, the differences between spectra from different clouds should reflect only the effects of the density distribution along the line of sight. The spectra are shown in Fig. 5.

Since the model F2 has the highest average density it has also the strongest emission in all transitions. The enlarged column densities of clouds F1 and F3 do increase the intensities of all transitions but increased self-absorption and increased line-widths are also evident.

Real clouds may have very low volume filling factors f and in many regions of massive star formation the volume filling factor has been estimated to lie in the range $f \sim$0.1-0.2 (e.g.
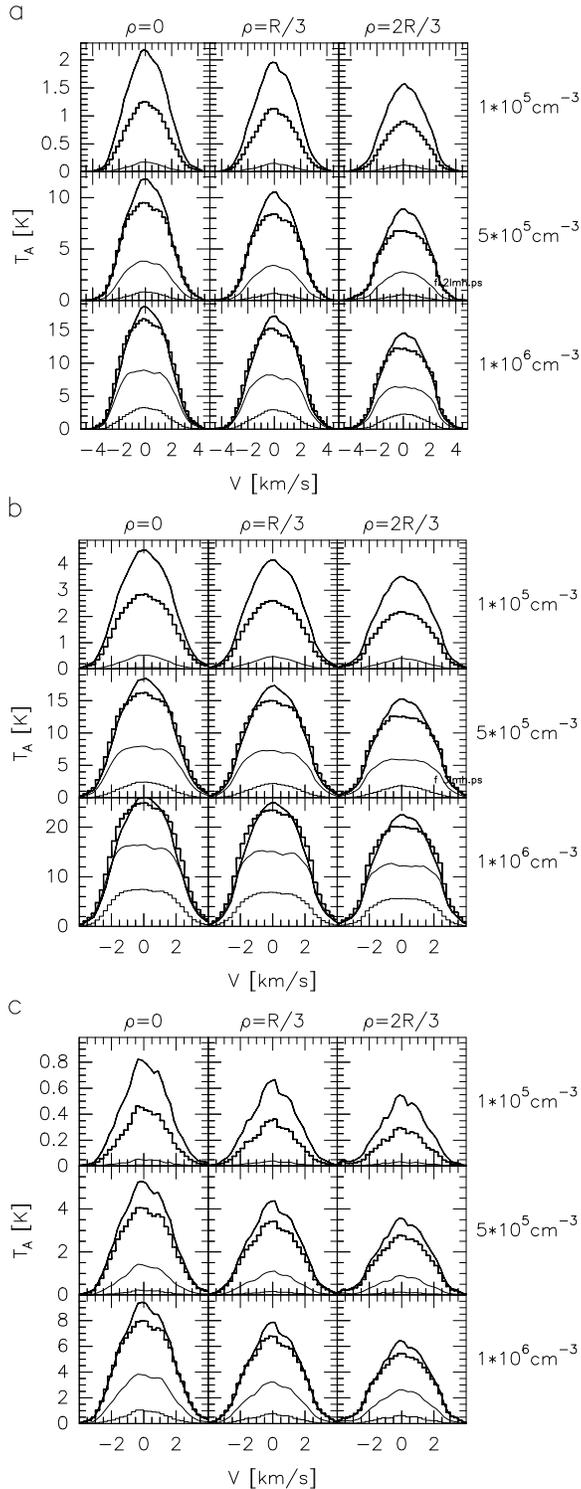
a

b

c

Fig. 3a–c. The CS spectra calculated from the clouds F1 (frame **a**), F2 (frame **b**) and F3 (frame **c**) with T_{kin}=40.0 K. The densities were scaled from 0.0 to $1.0 \cdot 10^5$ cm^{-3} (top row), from 0.0 to $5.0 \cdot 10^5$ cm^{-3} (middle row) and from 0.0 to $1.0 \cdot 10^6$ cm^{-3} (bottom row). On each row the first frame contains the spectra observed towards the centre of the cloud and the following frames contain spectra at distances of 1/3 and 2/3 times the cloud radius. The lines CS(7–6) (thin histogram), CS(5–4) (thin line), CS(2–1) (thick line) and CS(3–2) (thick histogram) are shown for each position
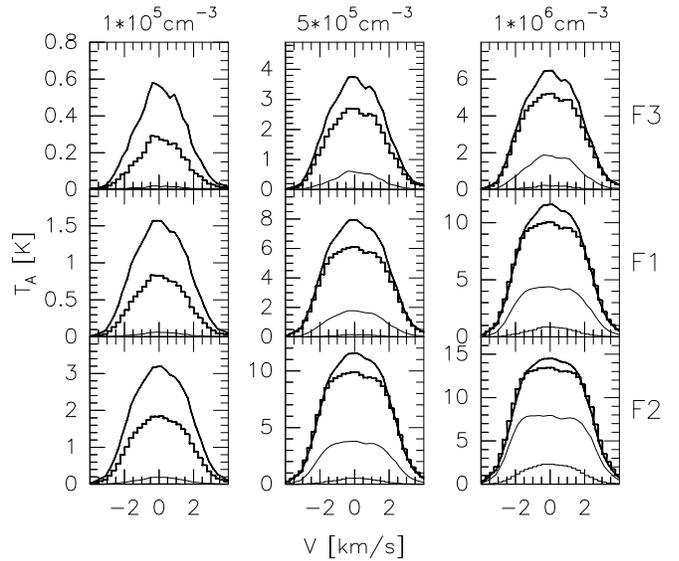

Fig. 4. The CS spectra calculated towards the central positions of the fractal clouds with T_{kin}=20 K. The maximum densities of the clouds were $1.0 \cdot 10^5$ cm^{-3} (first column), $5.0 \cdot 10^5$ cm^{-3} or $1.0 \cdot 10^6$ cm^{-3} (last column). The first row contains spectra from F3, the second from F1 and the third from F2. Transitions CS(2–1) (thick lines), CS(3–2) (thick histograms), CS(5–4) (thin lines) and CS(7–6) (thin histograms), are shown

Zhou et al. 1994; Mundy et al. 1986). Although the fractal model clouds have a large fraction of low density cells, the effective volume filling factor is still rather high. To study the effect of smaller f we modified the clouds by removing a number of randomly selected cells from the clouds. This procedure may also change the fractal dimension of the clouds. We selected only cloud F1 for this study. In Fig. 6 we show the spectra from F1 with the maximum density scaled to $5.0 \cdot 10^6$ cm^{-3}. The three frames show the spectra from the central position when the volume filling factor was set to 0.05, 0.15 and 0.4.

The volume filling factor has the expected effects. Although the density has been increased from Fig. 3a the lines are generally less self-absorbed. The lines become wider with increasing volume filling factor. Note that in the last frame all lines are much stronger than in Fig. 3a and the line profiles are still almost Gaussian. The low volume filling factor combined with the existence of macroturbulent motions seems therefore to be effective in reducing self-absorption. The changes in the volume filling factor have also affected the line ratios. The intensity of CS(2–1) clearly increases with increasing f while the relative intensity of CS(5–4) has dropped slightly.

The small-scale structure in the line profiles is entirely due to the macroturbulence. As the volume filling factor gets lower the spectra from individual cells are averaged with fewer other cells and the line profile appears 'clumpy'. This sub–structure is of course entirely dependent on the cell size used in the model cloud. Since the lines are emitted in different fashion from cells with different densities, the profiles of different transitions may
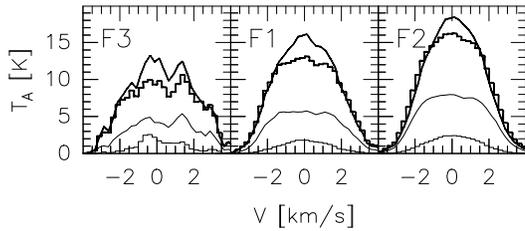
Fig. 5. The CS spectra calculated towards the central positions of the fractal clouds F3, F1 and F2 after the beam averaged column densities in the centre positions were adjusted to $7.9 \cdot 10^{14}\,\mathrm{cm}^{-2}$ by scaling the cloud sizes

Fig. 6. The CS spectra calculated towards the centre of the fractal cloud F1 after the volume filling factor was reduced by removing randomly selected cells. The volume filling factors f are 0.05 (leftmost frames), 0.15 and 0.4 (rightmost frames). The maximum density of the clouds was scaled to $5.0 \cdot 10^{6}\,\mathrm{cm}^{-3}$ (upper frames) and $1.0 \cdot 10^{6}\,\mathrm{cm}^{-3}$ (lower frames)

also deviate significantly from each other (see e.g. lines CS(2–1) and CS(7–6) in Fig. 6).

In Fig. 6 we show similar spectra from the cloud F1 with lower maximum density, $1.0 \cdot 10^{6}\,\mathrm{cm}^{-3}$. The 'noise' in the profiles of e.g. CS(5–4) seem a little higher than in the case of higher gas density. This probably reflects the fact that fewer cells have the densities required to emit these transitions.

5.1.2. Microturbulent clouds

It is also interesting to compare the calculations with the results from microturbulent models. In the previous calculations the microturbulence was only $\sigma_\mu = 0.2\,\mathrm{km\,s}^{-1}$ while the macroscopic random motions of the cells were mainly responsible for the observed linewidths.

In the following the clouds have no macroturbulence but the microturbulence has been increased to $\sigma = 1.5\,\mathrm{km\,s}^{-1}$. The linewidths should be comparable to the earlier calculations with macroturbulent clouds. In Fig. 7a we present calculations with model clouds that are, apart from the turbulence, exactly the same as in Fig. 3. The infall velocity still exists in the clouds so that the model is not purely microturbulent. The infall velocity is, however, much smaller than the linewidths.

The most important difference between Fig. 7a and the macroturbulent case is the marked increase in the self-absorption. In the microturbulent clouds the self-absorption features set in at lower densities, and at higher densities the spectra have clear absorption dips instead of being just flat-topped. With the absence of the noise from the macroturbulence and due to the increased self-absorption, the line asymmetry caused by the infall motion can also be clearly seen. All line intensities have remained approximately the same as in Fig. 3 and the differences are mainly linked to the increased absorption (e.g. cloud F2, lines CS(3–2) and CS(2–1)).

The results of microturbulent models corresponding to the macroturbulent ones presented in Fig. 4 are shown in Fig. 7b. These clouds have a kinetic temperature of $T_{\mathrm{kin}} = 20\,\mathrm{K}$. Here also the differences from the macroturbulent case are visible even at the lowest densities.

Comparison between microturbulent models with different kinetic temperatures has similarities with the previous comparison between macroturbulent models with different tempera-
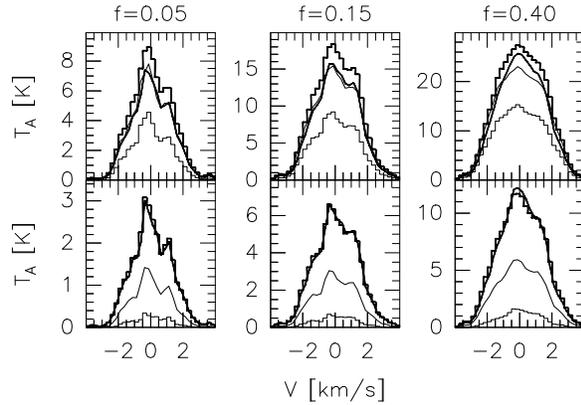
tures. The lowering of the temperature does not radically change the line ratios but e.g. the self-absorption of CS(2–1) has increased.

To see the effect of the volume filling factor more clearly we made also comparisons with some clouds with $f=1.0$. For this purpose we calculated the spectra for spherically symmetric, one-dimensional models. The clouds are divided into 30 shells, all with equal thickness. The density was set according to law $n \propto r^\alpha$ and scaled approximately to the same range as in the corresponding fractal cloud. The beam averaged column densities were calculated at the cloud centre as well as at distances corresponding to 1/3 and 2/3 of the radius of the three-dimensional cloud. The cloud parameters were modified in such a way that the column densities agreed to within 10% with the corresponding values from the three-dimensional fractal cloud. The clouds should therefore have similar large-scale density distributions as their three-dimensional counterparts. In Fig. 8 we show the spectra from the one-dimensional cloud corresponding to the three-dimensional model calculations shown in Fig. 6 (upper frames).

The correspondence between the column densities of the one-dimensional and the three-dimensional cloud cannot be exact since the density structure of a fractal cloud does not obey exponential laws. Also, the mass spectra of 1D and 3D clouds differ and therefore the differences in the calculated spectra are not just caused by differences in f. These complications must be kept in mind when comparisons are made between different models.

The self-absorption of the spectra in Fig. 8 is very strong even though the line intensities are similar to or lower than in the spectra from the three-dimensional clouds with similar column and volume densities. This can be seen as further evidence for the fact that clumpy clouds produce spectra with less self-absorption. However, direct comparison between the spectra is difficult as can be seen from e.g. the different line ratios. The
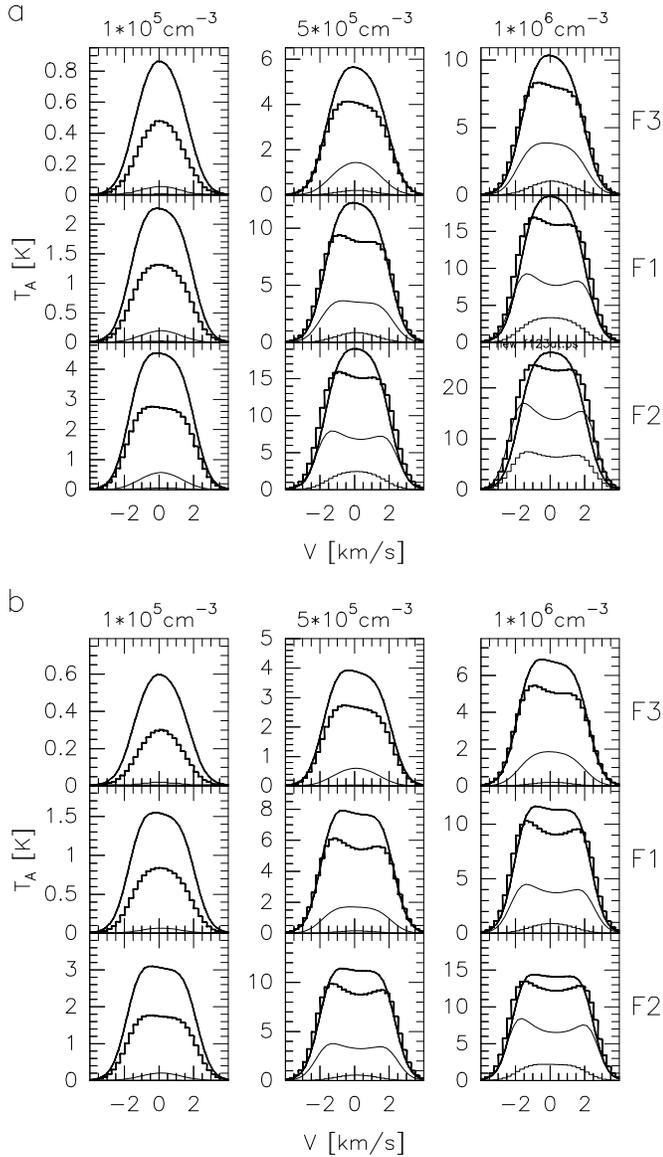
Fig. 8. Spectra calculated from spherically symmetric model clouds with T_{kin}=40 K. The beam averaged column densities are approximately the same as for the cloud F1 in Fig. 6 (upper frame). The density drops by a factor of 100 from the cloud centre to the surface. For the three models the centre densities are $3.0 \cdot 10^6 \, cm^{-6}$, $5.0 \cdot 10^6 \, cm^{-6}$ and $4.0 \cdot 10^6 \, cm^{-6}$ and the diameters of the model clouds divided by the diameter of the three-dimensional clouds are 1.1, 1.3 and 1.1. The density distributions were set according to $n \propto r^\alpha$ with α=-1.5 in frame **a**, α=-1.2 in frame **b** and α=-0.4 in frame **c**
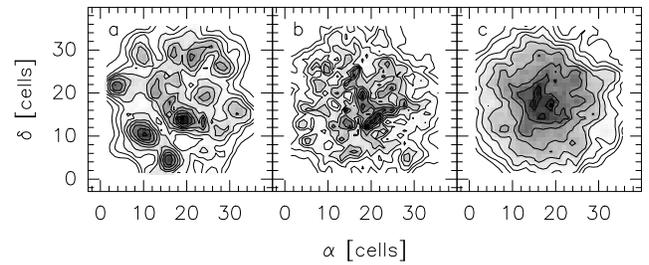
Fig. 9a–c. The column density maps of the model clouds T1 (frame **a**), T2 (frame **b**) and T3 (frame **c**) all created using the structure tree method. The contours are drawn at intervals 10% of the map maximum starting at 20%. The column density scale is arbitrary since the densities were always scaled before calculations

through the cloud in the direction of the cloud centre. The optical depths are calculated for the line centre. Note also that the values are calculated along a single line of sight and e.g. the column densities might vary significantly even between close positions.

5.2. Clouds created with structure trees

The column density maps of three clouds created with structure trees are shown in Fig. 9. The basic density distribution of the clouds and the added clumps is $n \propto r^{-0.5}$. Since the density distribution was also used as the probability distribution for the position of the sub-clumps the column density clearly peaks close to the centre of the maps. In all created clouds the density of each sub-clump is five times the density of parent clump.

Cloud T1 has a branching factor of η=5 and each clump has a size 0.5 times that of its parent. Due to the relatively coarse discretization there are only four levels in the structure tree and the smallest clumps have a diameter of 4.5 cells. Cloud T2 is similar to T1 except that it has a branching factor of 10 and the size ratio between sub-clumps and clumps is 0.3.

Fig. 7. a Spectra calculated with microturbulent models. The clouds are identical to those in Fig. 3 except that the macroscopic cell motions have been removed and the microturbulence increased correspondingly. The kinetic temperature is constant T_{kin}=40 K. The maximum densities of the clouds were $1.0 \cdot 10^5 \, cm^{-3}$ for the spectra in the first first column, $5.0 \cdot 10^5 \, cm^{-3}$ for the next column and $1.0 \cdot 10^6 \, cm^{-3}$ for the last column. The three rows correspond to fractal models F3, F1 and F2. **b** The corresponding spectra calculated with microturbulent model clouds with T_{kin}=20 K

differences in the mass spectra and the cloud sizes are clearly responsible for some of the differences.

5.1.3. Summary of the calculations with fractal cloud models

In Table 1 we list the parameters of all the fractal models for which the calculations were described in the previous chapters. The table lists also column densities and the optical depths
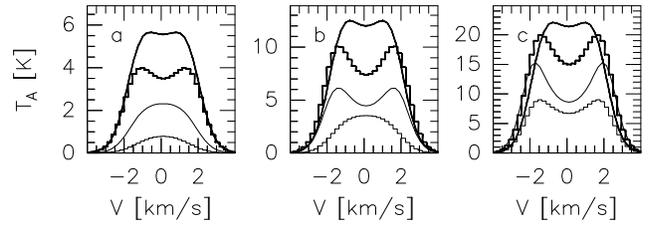
Table 1. The parameters of the fractal cloud models. The columns are: the model cloud (column 1), the maximum density in the cloud (column 2), kinetic temperature (column 3), column density N_{CS} towards the cloud centre (column 4), the optical depths in the line centre towards the cloud centre (columns 5–8) and the figure in which the spectra are shown (column 9)

Model	n_{max} (cm^{-3})	T_{kin} (K)	N_{CS} (cm^{-2})	Optical depths				Fig.
				$\tau(2-1)$	$\tau(3-2)$	$\tau(5-4)$	$\tau(7-6)$	
macroturbulent clouds								
F1	$1.0\cdot10^5$	40	$1.3\cdot10^{14}$	5.8	6.2	0.5	0.02	3a
F1	$5.0\cdot10^5$	40	$6.5\cdot10^{14}$	5.9	11.9	13.0	1.6	3a
F1	$1.0\cdot10^6$	40	$1.3\cdot10^{15}$	6.4	13.3	22.1	9.7	3a
F2	$1.0\cdot10^5$	40	$2.0\cdot10^{14}$	5.8	8.4	1.5	0.04	3b
F2	$5.0\cdot10^5$	40	$1.0\cdot10^{15}$	5.7	11.6	18.4	5.7	3b
F2	$1.0\cdot10^6$	40	$2.0\cdot10^{15}$	7.0	13.9	25.3	20.6	3b
F3	$1.0\cdot10^5$	40	$6.6\cdot10^{13}$	4.3	3.1	0.2	0.05	3c
F3	$5.0\cdot10^5$	40	$3.3\cdot10^{14}$	6.3	10.5	4.9	0.3	3c
F3	$1.0\cdot10^6$	40	$6.6\cdot10^{14}$	6.4	12.5	12.7	2.5	3c
F1	$1.0\cdot10^5$	20	$1.3\cdot10^{14}$	7.5	6.5	0.3	0.004	4
F1	$5.0\cdot10^5$	20	$6.5\cdot10^{14}$	11.1	18.1	11.3	0.4	4
F1	$1.0\cdot10^6$	20	$1.3\cdot10^{15}$	14.7	24.5	25.7	3.7	4
F2	$1.0\cdot10^5$	20	$2.0\cdot10^{14}$	8.2	9.6	0.8	0.01	4
F2	$5.0\cdot10^5$	20	$1.0\cdot10^{15}$	12.2	20.3	20.1	16.8	4
F2	$1.0\cdot10^6$	20	$2.0\cdot10^{15}$	18.4	30.4	35.1	11.1	4
F3	$1.0\cdot10^5$	20	$6.6\cdot10^{13}$	5.0	3.0	0.1	0.001	4
F3	$5.0\cdot10^5$	20	$3.3\cdot10^{14}$	10.0	13.4	3.6	0.09	4
F3	$1.0\cdot10^6$	20	$6.6\cdot10^{14}$	12.1	19.0	11.4	0.8	4
macroturbulent clouds with equal column densities								
F1	$5.0\cdot10^5$	40	$1.3\cdot10^{15}$	8.5	17.0	23.4	5.0	5
F2	$5.0\cdot10^5$	40	$1.3\cdot10^{15}$	5.7	11.6	18.4	5.7	5
F3	$5.0\cdot10^5$	40	$1.3\cdot10^{15}$	16.1	29.3	30.6	5.7	5
macroturbulent clouds with low volume filling factors								
F1	$5.0\cdot10^6$	40	$3.7\cdot10^{14}$	3.0	5.9	10.6	10.6	6
F1	$5.0\cdot10^6$	40	$1.1\cdot10^{15}$	4.9	9.7	17.6	17.3	6
F1	$5.0\cdot10^6$	40	$1.9\cdot10^{15}$	6.7	13.1	23.1	23.5	6
F1	$1.0\cdot10^6$	40	$7.4\cdot10^{13}$	1.0	2.3	4.1	2.0	6
F1	$1.0\cdot10^6$	40	$2.1\cdot10^{14}$	1.9	4.4	6.9	2.5	6
F1	$1.0\cdot10^6$	40	$3.8\cdot10^{14}$	2.5	5.6	9.5	4.0	6
microturbulent clouds								
F1	$1.0\cdot10^5$	40	$1.3\cdot10^{14}$	3.1	3.1	0.2	0.01	7a
F1	$5.0\cdot10^5$	40	$6.5\cdot10^{14}$	3.2	6.5	6.4	0.6	7a
F1	$1.0\cdot10^6$	40	$1.3\cdot10^{15}$	3.4	7.1	11.5	4.3	7a
F2	$1.0\cdot10^5$	40	$2.0\cdot10^{14}$	3.2	4.4	6.7	0.02	7a
F2	$5.0\cdot10^5$	40	$1.0\cdot10^{15}$	3.1	6.3	9.6	2.5	7a
F2	$1.0\cdot10^6$	40	$2.0\cdot10^{15}$	3.7	7.5	13.4	10.2	7a
F3	$1.0\cdot10^5$	40	$6.6\cdot10^{13}$	2.2	1.5	0.07	0.002	7a
F3	$5.0\cdot10^5$	40	$3.3\cdot10^{14}$	3.3	5.5	2.1	0.1	7a
F3	$1.0\cdot10^6$	40	$6.6\cdot10^{14}$	3.3	6.7	6.2	0.8	7a
F1	$1.0\cdot10^5$	20	$1.3\cdot10^{14}$	3.9	3.1	0.1	0.002	7b
F1	$5.0\cdot10^5$	20	$6.5\cdot10^{14}$	5.8	9.3	5.1	0.1	7b
F1	$1.0\cdot10^6$	20	$1.3\cdot10^{15}$	7.5	12.5	12.6	1.4	7b
F2	$1.0\cdot10^5$	20	$2.0\cdot10^{14}$	4.3	4.8	0.4	0.005	7b
F2	$5.0\cdot10^5$	20	$1.0\cdot10^{15}$	6.3	10.5	9.8	0.6	7b
F2	$1.0\cdot10^6$	20	$2.0\cdot10^{15}$	9.3	15.5	17.6	5.0	7b
F3	$1.0\cdot10^5$	20	$6.6\cdot10^{13}$	2.5	1.4	0.03	0.001	7b
F3	$5.0\cdot10^5$	20	$3.3\cdot10^{14}$	5.1	6.7	1.3	0.03	7b
F3	$1.0\cdot10^6$	20	$6.6\cdot10^{14}$	6.1	9.6	5.0	0.2	7b

Table 2. Parameters of the structure trees used to create the model clouds T1, T2 and T3. The branching factor η is the number of sub-clumps within a clump, N is the number of levels in the structure tree with the root cloud included as one of the levels and k_L is the ratio of the linear sizes between a sub-clump and a clump

cloud	branching factor η	number of levels N	size ratio k_L
T1	5	4	0.5
T2	10	3	0.3
T3	100	2	0.2

The last cloud, T3, has a branching factor of 100 and the structure tree has only two levels. The cloud consists therefore of 100 clumps with a radius of $\sim$3.6 cells. The clumps are generated preferentially close to the cloud centre with a probability $\sim r^{-0.5}$ when $r > 1.0$ cells, and a constant probability inside this radius. This means that in T3 the central region is practically filled with high density gas and the volume filling factor drops only close to the the cloud surface. The clumps are allowed to intersect but the density of the intersection is updated only once and therefore the density in the central region should be almost constant.

5.2.1. Clouds with macroturbulence

The amount of microturbulence was first set to σ_μ=0.2 km s^{-1} and the macroturbulence to σ_M=1.2 km s^{-1}. A small infall velocity was again added as v(r)=v$_0$ r$^{-\alpha}$, where α=0.5 and the infall velocity at the cloud surface v$_0$=0.15 km s^{-1}.

We present the spectra calculated towards the central positions of the clouds in Fig. 10a. The maximum densities of all clouds were scaled to 1.0·10^6, 5.0·10^6 and 1.0·10^7 cm^{-3}. The clouds have a size of 0.058 pc in all three dimensions. These clouds are therefore both smaller and denser than the fractal clouds.

One can again see large differences in the observed line ratios. The beam-averaged column densities towards the cloud centres were 7.59·10^{13} cm^{-2} for T1, 8.73·10^{13} cm^{-2} for T2, and 1.55·10^{14} cm^{-2} for T3 when the maximum density of the clouds was scaled to 1.0·10^6 cm^{-3}. When the structure tree has only two levels, as is the case for T3, the proportion of high density cells is rather high. As soon as the structure tree has more levels the density differences between the densest clumps and the ambient cloud become large and, since the densities in all clouds were scaled to the same range, clouds T1 and T2 have lower average densities. These differences are reflected in the relative intensity and the self-absorption of the line CS(7–6).

The highest density range used for the fractal clouds was the same as the lowest density range here i.e. from zero to 1.0·10^6 cm^{-3}. Comparing the corresponding spectra here and in Fig. 3 we notice that the line ratios have indeed remained about the same. For example models F3 and T3 seem to be very close to each other.

Despite the higher densities the optical depths are somewhat lower than in the fractal clouds. The optical depths of the models are listed also Table 3.
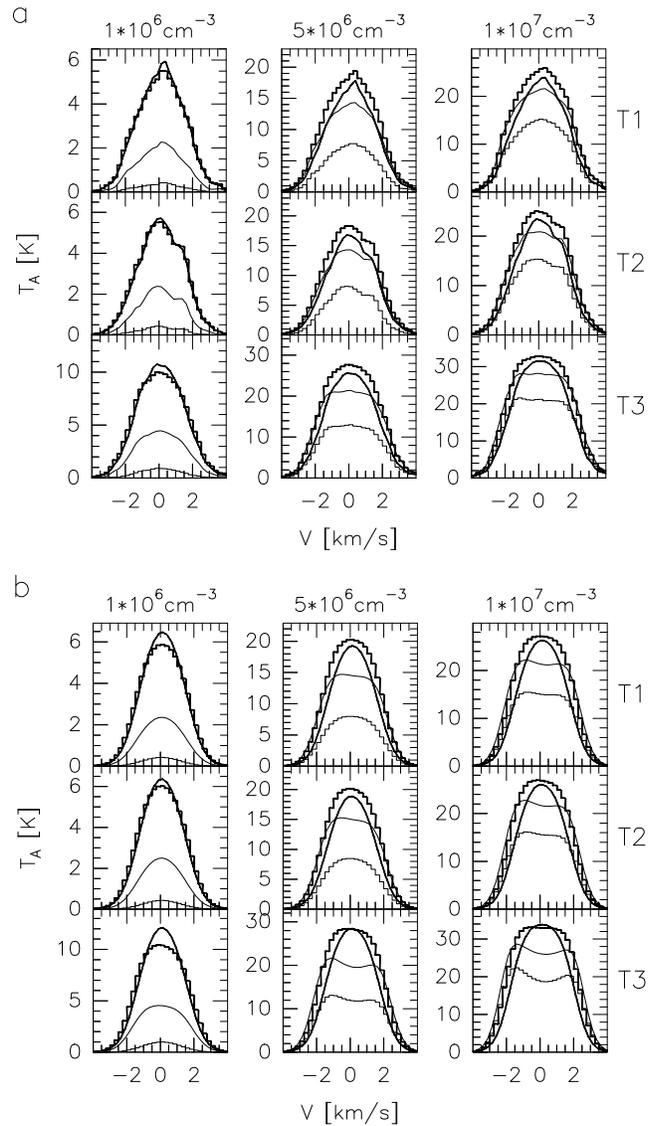

Fig. 10. a The CS spectra observed towards the central positions of the macroturbulent clouds created with structure trees. The kinetic temperature of the clouds is constant T$_{kin}$=40.0 K. The frames on the first row show spectra from the cloud T1, the second row from T2 and the third from T3. The maximum densities of the clouds were 1.0·10^6 cm^{-3} (first column), 5.0·10^6 cm^{-3} and 1.0·10^7 cm^{-3} (last column). Transitions CS(2–1) (thick lines), CS(3–2) (thick histograms), CS(5–4) (thin lines) and CS(7–6) (thin histograms), are shown. **b** Spectra calculated with microturbulent models. The clouds are identical to those in **a** except that the macroscopic cell motions have been eliminated and the microturbulence has been correspondingly increased

5.2.2. Microturbulent clouds

We show in Fig. 10b spectra calculated with microturbulent models where σ_μ=1.5 km s^{-1}. The infall velocity is the same as in the previous clouds so that the models are not purely microturbulent. The densities are scaled to the same ranges as in in Fig. 10a.

The same effects can be seen here as in Fig. 7a i.e. the spectra show increased self-absorption and larger line-widths compared
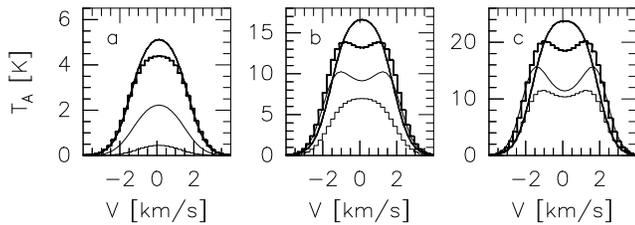
Fig. 11. The CS spectra observed towards the centre of a spherically symmetric model cloud with $n \propto r^{-1.0}$. The cloud size has been scaled in such a way that the beam averaged column densities are similar to those in the cloud T2, Fig. 10a. The densities were scaled to the range from zero to $1.0 \cdot 10^6$ (frame **a**), $5.0 \cdot 10^6$ (frame **b**) and $1.0 \cdot 10^7$ cm^{-3} (frame **c**)

with the macroturbulent case. Changes in the line ratios are also mainly correlated with the self-absorption.

In Fig. 11 we show again some spectra calculated with one-dimensional models. The model cloud consists of 30 spheres of equal thickness. The densities are scaled to the same ranges as in the three-dimensional cloud T2 in Fig. 10a. The radial density dependence is $n \propto r^{-1.0}$ and the cloud sizes have been scaled so that the beam-averaged column densities are similar at the cloud centres as well as at distances of 1/3 and 2/3 of the radius of the three-dimensional cloud. The column densities of the 1D and 3D clouds agree within a few percent in all three positions.

The lines calculated from the 1D cloud are again very strongly self-absorbed compared even with the microturbulent spectra. The intensities of the lines are generally similar in the 1D and the 3D clouds. This seems to indicate that the correspondence between the 1D and 3D models is rather good. The strong self-absorption is, however, partly due to the existence of low density gas with the density systematically dropping towards the cloud surface. Together with microturbulent velocity structure this gives the best conditions for self-absorption.

5.2.3. Summary of the clouds created with structure trees

In Table 3 we list the parameters of the model clouds created using structure trees. The basic models T1, T2 and T3 have different density distributions and the actual model clouds were created by scaling these densities and by setting different values of turbulence etc. The table lists also the column densities and the optical depths through the clouds calculated along a single line of sight. The optical depths are the values for the line centre.

6. Discussion

The number of rotational levels included into the calculations was 11. This is sufficient since the number of molecules at the first omitted excitation level was found to be insignificant for all density and temperature combinations used. This was confirmed by scaling the densities in the clouds F2 and T3 to the highest density intervals used in the previous calculations and by repeating these calculations with 13 excitation levels. Towards the centre of the fractal cloud F2 the number of molecules on

the excitation level $J = 11$ (averaged over the line of sight) was already about $1.0 \cdot 10^{-4}$ times less than the number of molecules on the level $J = 3$. Similarly for cloud T3, with the average density close to $1.0 \cdot 10^7 \text{cm}^{-3}$, the population of the level $J = 11$ was about 500 times less than that of the most populated levels.

The collisional coefficients were taken from Green & Chapman (1978). There exists, however, also a more recent set of coefficients given in Turner et al. (1992). We repeated the calculations of the models F2 and T3 with the new coefficients using again the highest density ranges employed in the previous calculations. The differences in the line intensities were at least below 0.3 K i.e. no clear differences could be seen in the figures. Also the line profiles remained unchanged. Therefore, the choice of the collision coefficients does not affect the results of this paper.

6.1. Effects of discretization

Before we can draw any definite conclusions from e.g. the comparison of one-dimensional and three-dimensional models we must first consider the effects that the discretization has on the computed spectra. In one-dimensional clouds we can easily use a very fine grid size and thus make sure that the results are not affected by the discretization. For a three-dimensional cloud this is not always possible for practical reasons.

Each cell should be so small that the excitation conditions are approximately constant within the cell. In Fig. 12 we show a series of figures of the excitation temperature distributions in one-dimensional clouds with different sizes and densities. Compared with the physical parameters of a single cell these can give us an idea in which conditions the discretization may affect the outcome of the radiative transfer calculations. In fact this is the worst case scenario since in the three-dimensional cloud each cell is surrounded by similar cells and therefore the excitation conditions are more homogeneous. In the following we shall call the one-dimensional model clouds 'cells' since the results are compared with individual cells of the three-dimensional clouds.

The upper frames of Fig. 12 correspond to a cell size that is $\sim 10\%$ larger than the cell sizes in model clouds T1, T2 and T3. At the density of $5.0 \cdot 10^6$ cm^{-3} there are already noticeable changes in the excitation temperatures. For the transitions 5–4 T_{ex} drops at the surface of the cell about 1 K from the value at the centre. However, since the effect is much smaller for cells embedded in a cloud we may still conclude that the chosen cell size does not cause significant errors to the line profiles calculated from the three-dimensional clouds. Also the optical depths of all cells in the clouds T1, T2 and T3 were less than 1.0.

The cell size used in connection with the fractal clouds was much larger. For example, in cloud F2 the optical depth of the transition CS(5–4) was in some cells over 2.0 when the maximum density of the cloud was scaled to $1.0 \cdot 10^6$ cm^{-3}. The lower frames of Fig. 12 correspond to a cell size $\sim 13\%$ larger than in the fractal clouds. From this figure we can see that the drop in the excitation temperature of the 5–4 transition is already about 4 K when the density of the cell is $5.0 \cdot 10^6$ cm^{-3}. In a cloud

Table 3. The parameters of model clouds in which the density distribution was generated using structure trees. The columns are: the model cloud (column 1), the maximum density in the cloud (column 2), kinetic temperature (column 3), column density N_{CS} towards the cloud centre (column 4), the optical depths in the line centre towards the cloud centre (columns 5–8) and the figure in which the spectra are shown (column 9)

Model	n_{max} (cm^{-3})	T_{kin} (K)	N_{CS} (cm^{-2})	Optical depths $\tau(2-1)$	$\tau(3-2)$	$\tau(5-4)$	$\tau(7-6)$	Fig.
macroturbulent clouds								
T1	$1.0 \cdot 10^6$	40	$1.5 \cdot 10^{14}$	1.1	2.6	1.9	0.3	10a
T1	$5.0 \cdot 10^6$	40	$7.4 \cdot 10^{14}$	1.7	3.8	7.0	4.9	10a
T1	$1.0 \cdot 10^7$	40	$1.5 \cdot 10^{15}$	2.7	5.6	10.3	9.7	10a
T2	$1.0 \cdot 10^6$	40	$1.1 \cdot 10^{14}$	0.9	1.7	1.2	0.1	10a
T2	$5.0 \cdot 10^6$	40	$5.6 \cdot 10^{14}$	1.2	2.6	4.6	3.2	10a
T2	$1.0 \cdot 10^7$	40	$1.1 \cdot 10^{15}$	1.9	3.8	6.7	6.3	10a
T3	$1.0 \cdot 10^6$	40	$2.5 \cdot 10^{14}$	1.3	2.8	2.9	0.4	10a
T3	$5.0 \cdot 10^6$	40	$1.2 \cdot 10^{15}$	2.2	4.5	8.1	7.3	10a
T3	$1.0 \cdot 10^7$	40	$2.5 \cdot 10^{15}$	3.6	7.1	12.6	12.5	10a
microturbulent clouds								
T1	$1.0 \cdot 10^6$	40	$1.5 \cdot 10^{14}$	1.1	2.1	1.2	0.1	10b
T1	$5.0 \cdot 10^6$	40	$7.4 \cdot 10^{14}$	0.8	1.6	2.7	2.7	10b
T1	$1.0 \cdot 10^7$	40	$1.5 \cdot 10^{15}$	1.6	3.1	5.5	5.3	10b
T2	$1.0 \cdot 10^6$	40	$1.1 \cdot 10^{14}$	0.9	1.6	0.9	0.06	10b
T2	$5.0 \cdot 10^6$	40	$5.6 \cdot 10^{14}$	1.2	2.6	4.1	2.5	10b
T2	$1.0 \cdot 10^7$	40	$1.1 \cdot 10^{15}$	1.7	3.5	6.1	5.3	10b
T3	$1.0 \cdot 10^6$	40	$2.5 \cdot 10^{14}$	1.0	2.3	2.4	0.3	10b
T3	$5.0 \cdot 10^6$	40	$1.2 \cdot 10^{15}$	1.8	3.8	6.8	6.2	10b
T3	$1.0 \cdot 10^7$	40	$2.5 \cdot 10^{15}$	3.1	6.0	10.7	10.5	10b

with the volume filling factor ~ 1 this change in the excitation conditions is distributed over several cells and the effects of the discretization are again insignificant (see e.g. Fig. 1 in Park & Hong 1995). On the other hand, in e.g. Fig. 6a the cloud has both a high density and a small volume filling factor. This means that many cells are subjected only to the background radiation and the excitation temperatures of the upper transitions should drop at the cell surface. Since this is not possible there cannot be any self absorption within the cell either, i.e. the large cell size reduces the amount of self absorption in the calculated spectra. The volume filling factor 0.05 would mean, on the average, only a few non-empty cells in each line of sight through the cloud composed of $36 \times 36 \times 36$ cells. Because of the way the fractal clouds were created most of the mass is concentrated near the cloud centre and the volume filling factor is also significantly higher there. On the other hand, near the cloud surface the cells generally have very low optical depths. These factors may partly reduce the effects of the large cell size. However, these results should already be treated with some caution.

We have assumed a constant kinetic temperature for all clouds. If the cloud were subjected to some external heating mechanism, the kinetic temperatures of the clumps should increase towards the surface and the excitation temperatures of most lines would be more constant. At lower densities, however, the excitation temperature of the 2–1 transition increases towards the surface. Therefore the discretization will produce some errors in any case.
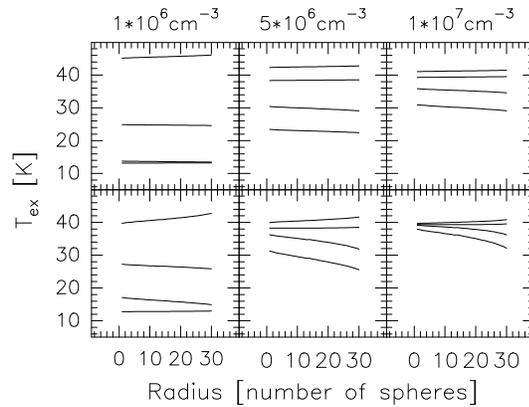

Fig. 12. The radial dependence of the excitation temperature in spherical clumps subjected to background radiation only. In each frame the lines from top to bottom show the excitation temperatures of the transitions 2–1, 3–2, 5–4 and 7–6. The diameter of the cells is 0.0019 pc for the upper frames and 0.0075 pc for the frames on the lower row. The constant densities of the cells are $1.0 \cdot 10^6$ cm^{-3} (leftmost frames), $5.0 \cdot 10^6$ cm^{-3} and $1.0 \cdot 10^7$ cm^{-3} (rightmost frames)

6.2. Effects of clumpiness: line profiles and intensities

The comparison of the three-dimensional clouds of Fig. 6 (T2 in Fig. 10a) and the one-dimensional clouds of Fig. 8 (Fig. 11) shows very clearly the effect that the density distribution has

on the observed line profiles. The self-absorption is stronger in the 1D-clouds and it is also enforced by the density structure which causes a drop in the excitation temperatures towards the cloud surface. However, both the 1D- and the 3D-clouds have approximately similar large scale density distributions. Clearly the clumpy cloud structure and the macroturbulence are the key factors causing the observed differences.

The spectra of the 1D-clouds have somewhat lower intensities than the spectra of the corresponding 3D-clouds even if the effect of the self-absorption is taken into account. This effect which is particularly clear at higher densities illustrates some of the difficulties in making comparisons between different kinds of models. The range of densities and the column densities averaged over all four beam sizes were about the same in both 1D- and 3D-clouds. As the 3D-clouds effectively have $f < 1.0$ the 1D-clouds with the same column densities must have lower densities in the cells. Therefore lower line intensities are observed in 1D-clouds as compared to 3D-clouds with the same column density.

Clouds F1, F2 and F2 have different distributions of cell densities (see Fig. 2). In F3 the majority of cells have a relatively low density while in F2 the proportion of dense cells is much higher. In general, these differences cause similar changes in the observed spectra as the volume filling factor. The effect of lowering the cell densities is not necessarily the same as that of lowering the volume filling factor, however. On the contrary, low density can also mean low excitation temperatures and this may in turn lead to increased self-absorption i.e. the effect might be quite the opposite to that of a low volume filling factor. In Fig. 13 we show the spectra from three clouds with cells of two densities. In each cloud half of the cells have a density of $5.0 \cdot 10^6$ cm^{-3} and the other half a density of $5.0 \cdot 10^4$ cm^{-3} (Fig. 13, frame **a**), $2.5 \cdot 10^5$ cm^{-3} (Frame **b**) or $1.0 \cdot 10^6$ cm^{-3} (Frame **c**). The figure shows that the denser cells are responsible for the major part of emission in all cases since the differences between the models are relatively small. It can also be seen that lowering the density of part of the cells has indeed lead to decreased self-absorption e.g. in CS(5–4) and CS(7–6). Therefore, the clumpy structure seems to be able to reduce the self-absorption when the density contrast between the clumps and the interclump material is modest. Note also that the line intensities have remained about the same in all three cases. The intensity of e.g. the 5–4 transition decreases, however, with increasing column density while the intensity of the optically thinner 2–1 transition increases.

If the maximum density of the clouds is scaled to the same value and the differences in the cell density distributions are allowed to modify the total column density, the amount of self absorption increases with the column density (see Figs. 3 and 4). On the other hand, in Fig. 5 the column densities are identical but the cloud sizes are correspondingly different. The effect of the cell density distribution is quite clear, i.e. very different line intensities are observed in e.g. clouds F1 and F2. This shows, once again, the uncertainty in determining the column density without a detailed knowledge of the actual density structure.
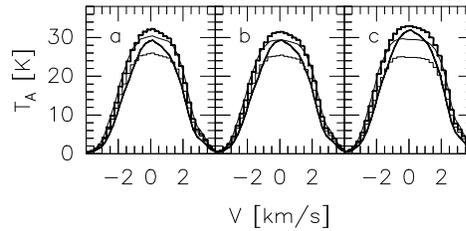

Fig. 13a–c. The spectra from clouds with the cells having only two possible density values. Half of the cells have a density of $5.0 \cdot 10^6$ cm^{-3}. The density in the other half is shown in frame **a** $5.0 \cdot 10^4$ cm^{-3}, in frame **b** $2.5 \cdot 10^5$ cm^{-3} and in frame **c** $1.0 \cdot 10^6$ cm^{-3}. The kinetic temperature is 40 K and the cloud size is the same as for e.g. T1

6.3. Effects of clumpiness: line ratios

The line ratios depend mostly on the temperature and the average density, and the differences between different clumpy density distributions are small. The density distribution is still important since it affects the self-absorption and in this respect the differences between e.g. the clumpy models and the spherically symmetric models were very large.

The line ratios depend therefore also on the actual distribution of the gas, the turbulence and the velocity field. As the lines become optically thick, reducing the volume filling factor affects the observed maximum antenna temperature only slightly. On the other hand, an increase in the column density may even reduce the peak line intensity because of the self-absorption. Since the intensity of the optically thin lines is directly proportional to f, the clumpy structure has a strong influence on the line ratios. Fig. 6a is a good example of this and the similar effect can be seen in Fig. 13.

There are some differences between the different fractal models in Fig. 3. The differences are not very large, however, and can be explained by differences in the mean densities and the self-absorption effects caused by the different column densities. Compared with the fractal clouds the line ratios observed from model clouds created with the structure tree statistics are more similar to each other. This is natural since all clumps in the tree models have the same density distribution, although at different size scales, and therefore the distributions of the cell densities are similar. The column densities of the tree models fall into a narrower range than those of the fractal models.

The column density maps of the fractal clouds and the clouds created with structure trees are very different. The spectra of e.g. F3 in Fig. 3c and T3 in Fig. 10 have, however, comparable line intensities. In order to see the effects of the model according to which the clumpy structure is generated we scaled the cloud F1 down by a factor of 4. The physical size of the cloud, 0.058 pc in each dimension, is then the same as the size of the clouds generated using structure trees. The spectra are shown in Fig. 15a. Comparing these spectra with e.g. the corresponding spectra from the cloud T3 one can see that the differences are very small. This seems to indicate that the actual method used to generate the the clumpy structure is only of secondary impor-
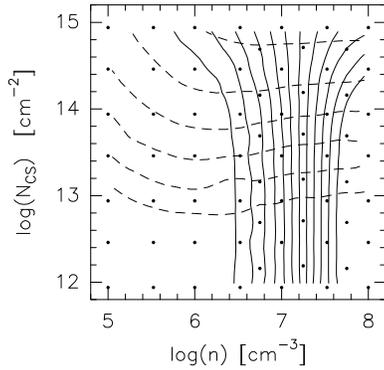
Fig. 14. The peak antenna temperature of CS(2–1) (dashed lines) and the ratio between CS(7–6) and CS(2–1) lines (solid lines) as the function of maximum density in the cloud and the beam averaged column density. The calculations have been made with the fractal cloud F1 using a beam with FWHM equal to one sixth of the cloud diameter

tance and the line ratios are mainly determined by the overall distribution of the cell densities. The result is encouraging since it indicates that real clouds can be modeled with clumpy density distributions even though the exact nature of the small scale clumpiness is still unknown.

The line ratios in clumpy clouds should be different from the line ratios in microturbulent clouds or LVG models and e.g. the column densities predicted by clumpy models should be higher. In order to study these differences we scaled the density and size of cloud F1 and produced spectra from a large density and column density range. The results for $T_A(2–1)$ and the ratio $T_A(7–6)/T_A(2–1)$ are shown Fig. 14 as the function of the maximum cloud density and the beam averaged column density.

This graph can be compared with the LVG calculations of Zinchenko et al. 1994 (their Fig. 22). Our y-axis is the total column density integrated over the line and not $N/\delta V$ as in the LVG graphs. In the optically thin case the FWHM of the CS line was in our calculations about 3.5km s^{-1}. Therefore e.g. the column density value $N = 1.0 \cdot 10^{14} \text{cm}^{-3}$ corresponds to $N/\Delta V = 0.27 \cdot 10^{14} \text{cm}^{-3}/\text{km s}^{-1}$ in the line centre. When this difference is taken into account our model predicts only slightly higher column densities than the LVG model. This may indicate that the cloud F1 is not clumpy enough (see Fig. 2b) for the effects of clumpiness to show more clearly.

From Fig. 2a we can see that the mean density of the cloud F1 is around 20% of the maximum value. The predicted mean densities are therefore lower than the densities predicted by the LVG model. The differences are larger at higher densities where the lines become saturated. At low column densities the value $T_A(7–6)/T_A(2–1)=1.2$ is reached in the LVG model at density $3 \times 10^7 \text{cm}^{-3}$ while the corresponding mean density in our model is lower by a factor of three.
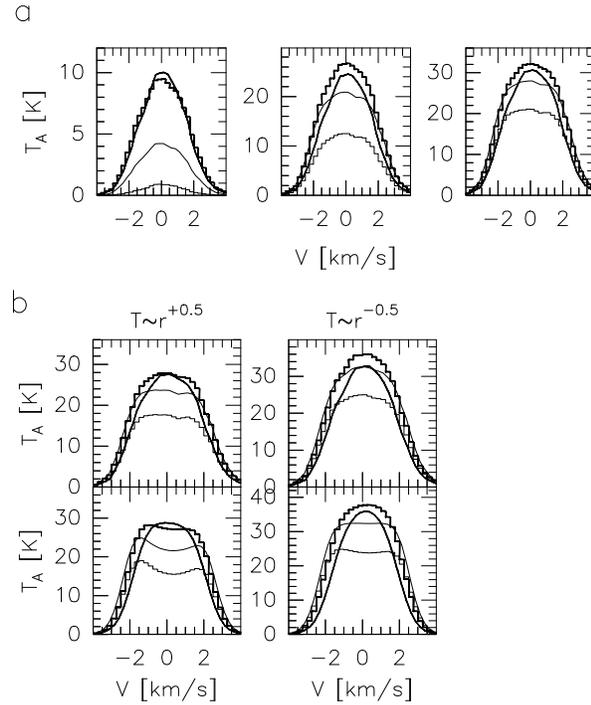

Fig. 15. a The spectra from the cloud F1 after scaling the size down to the size of the clouds generated with a structure-tree. The maximum densities of the clouds are $1.0 \cdot 10^6 \text{cm}^{-3}$, $5.0 \cdot 10^6 \text{cm}^{-3}$ and $1.0 \cdot 10^7 \text{cm}^{-3}$ for the subframes from left to right. The kinetic temperature is 40 K. **b** The spectra from cloud F1 with maximum density scaled to $1.0 \cdot 10^7 \text{cm}^{-3}$ after the kinetic temperature was modified. The radial dependence of the kinetic temperature was first set according to $r^{+0.5}$ (leftmost subframes) or $r^{-0.5}$ (rightmost subframes). The temperatures were then scaled to range from 30 K to 60 K. Upper subframes show the spectra from the macroturbulent clouds and the lower frames show spectra from the corresponding microturbulent clouds. The maximum density was $1.0 \cdot 10^7 \text{cm}^{-3}$ for all clouds

6.4. Effects of kinetic temperature distribution

We have so far assumed in all our calculations a constant kinetic temperature. This is of course not true for real interstellar molecular clouds. The kinetic temperature may either increase or decrease with distance from the cloud centre depending on strengths of the internal and external heating mechanisms. The temperature structure can change both the line ratios and the line profiles and e.g. the self-absorption features are highly dependent on the temperature distribution.

At this stage, we have not carried out detailed investigations of these effects. Instead, we shall present only one example that shows some of the qualitative effects involved. The kinetic temperatures of the cloud in Fig. 15a were modified with the temperatures either increasing or decreasing towards the cloud centre according to exponential laws $T_{kin} \sim r^{-0.5}$ and $T_{kin} \sim r^{0.5}$. The temperatures were then scaled to the ranges 30–60 K. The spectra towards these two model clouds are shown in Fig. 15b together with spectra from the corresponding microturbulent

clouds. These spectra can be compared also with the constant temperature model in Fig. 15a with T_{kin}=40.0 K.

The intensities in Fig. 15b are higher in rightmost frames since in these cases the temperature in the dense centre region is higher. For this reason the line ratios are somewhat different. As expected, the self-absorption is stronger in clouds where the kinetic temperature drops towards the cloud surface. For the line profiles the differences between the microturbulent and macroturbulent models are larger, however.

7. Summary

We have developed a new program for solving the radiative transfer problem in molecular clouds. The density distributions of the clouds are created either with fractal models or with the aid of structure trees. Based on theoretical considerations and the results from the test runs we have concluded that:

1. quasirandom numbers should be used in the simulation instead of pseudorandom numbers
2. the execution times can in some cases be dramatically reduced with a simple acceleration method involving the changes of the population levels
3. it may be necessary to reset the random number generators after each iteration in order to be able to follow the convergence; this can usually be done without endangering the correctness of the solution
4. in clouds with large density fluctuations or high optical depths our simulation method B should be more effective than the traditional Monte Carlo simulation

We have calculated spectra from different types of clumpy clouds and compared the results with the results from simple spherically symmetric cloud models. These results have confirmed that

1. the clumpy cloud structure and especially the existence of macroturbulence are needed to explain the general lack of self-absorption in the observed molecular spectra
2. apart from the mass spectrum of the clumps the radiative transfer properties of the clouds are not strongly dependent on the way the model clouds are generated
3. the estimates of column densities are very uncertain without detailed knowledge of the (clumpy) density distribution

In a forthcoming article we shall use our three-dimensional cloud models to analyze CS and $C^{34}S$ measurements of southern massive star forming regions (Juvela 1996). The derived physical parameters will be compared with the values calculated assuming LTE and with LVG models.

Appendix A: the details of the simulation methods

The cloud is divided into a number of cells and the radiation field is simulated with a number of photon packages. As a package goes through a cell the number of absorbed photons is calculated and registered by a counter in the cell. These counters are later used in the equilibrium equations to represent the number of induced transitions.

There are two methods for carrying out the simulation part of the calculations. The pseudocode for handling one photon packege is for the simulation method A (without the reference field):

1. generate a photon package with random position and random direction inside the cloud (or at the cloud boundary); initialize the photon package assigning to it a number of photons which is the number of real photons emitted by the cell (or the background) in one second divided by the expected number of photon packages generated in the cell (at the cloud boundary) during one iteration
2. repeat the following steps (a) to (c) until the package exits the cloud
   (a) move the package to the next cell boundary in the original direction
   (b) using the distance traveled within the cell calculate the optical depth along the trajectory
   (c) remove the number of absorbed photons from the package and add to a counter in the cell

The corresponding code for method B is:

1. generate a random position and random direction for a photon package at the cloud boundary; initialize the photon package assigning to it a number of photons which is the number of real photons emitted by the background in one second divided by the total number of photon packages generated during one iteration
2. repeat the following steps (a) to (d) until the package exits the cloud
   (a) move the package to the next cell boundary in the original direction
   (b) using the distance traveled in the cell calculate the optical depth along the trajectory
   (c) remove the number of absorbed photons from the package and add to a counter in the cell
   (d) calculate the number of photons emitted by the cell during one iteration, divided by the estimated number of photon packages going through the cell during one iteration and
      – calculate the fraction of these photons that is absorbed within this cell and add to counters in the cell
      – add the rest of these photons to the photon package

The level populations are assumed to be the same for all molecules within a cell. However, because of the turbulence and kinetic motions each cell contains molecules with different velocities and the excitation conditions may change with velocity. For example, in a collapsing cloud (if the local linewidth is large enough) each cell contains both molecules moving inwards and outwards and these should probably have different excitation temperatures. These effects are usually ignored and we do not consider them either. Since proper handling of such effects would increase the computational burden by at least one

order of magnitude such calculations are currently not practical for three-dimensional models.

In the following sections we list the equations implemented in the simulation program. These will also highlight the difference between our two simulation methods. Some of the equations can also be found in Bernes (1979) but are given here for reference.

A.1. Basic equations

In the following the excitation levels are marked with indices i and j, and levels u and l are such that $l = u - 1$.

The number of photons emitted in transition $u \rightarrow l$, divided by the volume of the emitting cell is

$$n_{ul}^\nu(\nu) = n_j A_{ul} \phi(\nu). \tag{A1}$$

and the number of photons coming from outside the cloud in one channel

$$n_{bg}^\nu = \frac{2\pi\nu^3}{c^3} \frac{\Delta v A}{e^{h\nu/kT_{bg}} - 1}, \tag{A2}$$

where Δv is the channel width in velocity and A the surface area. The emission profile $\phi(\nu)$ depends on the local gas properties: thermal motions and the microturbulence σ_μ. The optical depth of transition u$\rightarrow l$ over the distance s is

$$\tau = \frac{h\nu_{ul}}{4\pi}(n_l B_{lu} - n_u B_{ul})\phi(\nu)s. \tag{A3}$$

The absorption profile $\phi(\nu)$ is assumed to be the same as the emission profile and Gaussian in shape. The profiles of all transitions are also assumed to be separated from each other in frequency. As n^ν photons with the frequency ν travel a distance s, the number of induced upward transitions divided with the number of molecules on the lower level is

$$S_{lu} = \frac{h\nu}{4\pi}\phi(\nu)n_l B_{lu} n^\nu(\nu)\frac{s}{V}\frac{1 - e^{-\tau}}{\tau}. \tag{A4}$$

The total number of absorptions in one second per one molecule is marked S_{ij} and the equilibrium equations become

$$n_i \sum_j (A_{ij} + S_{ij} + C_{ij}) = \sum_j n_j(A_{ji} + \frac{g_i}{g_j}S_{ij} + C_{ji}). \tag{A5}$$

There are m equations of which only $m-1$ are linearly independent. One of the equations is replaced with $\sum_{i=1}^m n_i = n$, where n is the total number density of the molecule. The level populations can now be solved, since C_{ij} and A_{ij} are assumed to be known and S_{ij} are a result of the simulation. The simulation is continued using these new population values.

A.2. The use of a reference field

The random fluctuations of the results can be reduced by letting the photon packages represent only the difference between the real radiation field and some reference field corresponding to a constant temperature. The use of a reference field requires

changes to the calculations of interactions between photons and gas as well as the equilibrium equations (see also Bernes 1979).

The reference field corresponds a thermodynamic equilibrium at some temperature T_R. Let the number of real photons be n_ν^T and the number of photons corresponding to the reference field n_ν^R. The numbers of photons emitted from a cell with volume V in a transition $u \rightarrow l$ within a frequency $\Delta\nu$ are

$$
\begin{aligned}
n_\nu^T &= A_{ul}n_u V \Delta\nu\phi(\nu) \\
n_\nu^R &= A_{ul}n_l \frac{g_u}{g_l}e^{-\frac{h\nu}{kT_R}}V\Delta\nu\phi(\nu),
\end{aligned} \tag{A6}
$$

and photons from the background on an area of A,

$$
\begin{aligned}
n_\nu^T &= \pi A I_\nu(T_{bg})\frac{\Delta\nu}{h\nu}\phi(\nu) \\
n_\nu^R &= \pi A I_\nu(T_R)\frac{\Delta\nu}{h\nu}\phi(\nu).
\end{aligned} \tag{A7}
$$

As a photon package passes the distance s through a cell, we add to counters the number of absorption events

$$dS_{ij}(\nu) = \frac{h\nu}{4\pi}\phi(\nu)B_{lu}\left[n^T\frac{1 - e^{-\tau}}{\tau} - n^R\frac{1 - e^{-t}}{t}\right]\frac{s}{V}. \tag{A8}$$

Actually the counters contain these values integrated over the frequency. In this equation t is the optical depth of the cell for the reference photons

$$t = \frac{h\nu}{4\pi}n_l B_{lu}(1 - e^{-\frac{-h\nu}{kT_R}})s\phi(\nu). \tag{A9}$$

During the simulation only the difference between the real absorptions and the absorptions due to the reference field is calculated. The reference field which was previously subtracted is now added back in the equilibrium equations

$$n_i \sum_j (A_{ij} + B_{ij}I_\nu(T_R) + C_{ij} + S_{ij}) =$$

$$\sum_j \left[n_j(A_{ji} + B_{ji}I_\nu(T_R) + C_{ji} + S_{ji})\right]. \tag{A10}$$

Since the absorption counters S_{ij} depend on n^T and n^R calculated in the emitting cell the reference temperature that is used here must be the same, i.e. the reference temperature must be the same in all cells.

Instead of using a fixed reference temperature one can use as the reference the level populations from the previous iteration. The number of photons and the optical depth are calculated for the reference field in just the same way as for the true photons but using the level populations of the previous iteration (see Choi et al. 1995). In this way one does not have to specify reference temperatures and the reference field automatically gets close to its correct value as the iterations converge thereby minimizing the noise. On the other hand, one is forced to store the level populations of two iterations. The added memory requirement may be a problem with large three-dimensional models.

A.3. Photons absorbed in the emitting cell

The previous equations apply only to normal Monte Carlo– simulation (method A). In method B, however, photons are added to passing photon package only at the borders of the cells. If the optical depth of the cell is not very small the photons absorbed within the emitting cell must be treated explicitly and Eq. A8 must be modified. Firstly, by integrating over the photon path the number of new photons emitted from the cell is

$$n_+^{\mathrm{T}} = n_u A_{ul} V \frac{1 - e^{-\tau}}{\tau} \phi(\nu) \tag{A11}$$

for the exiting package. Similarly for the reference field

$$n_+^{\mathrm{R}} = n_l A_{ul} V \frac{g_u}{g_l} e^{-\frac{h\nu}{kT_\mathrm{R}}} \frac{1 - e^{-t}}{t} \phi(\nu). \tag{A12}$$

Since many rays pass the same cell during each iteration step, the numbers must also be weighted accordingly. When the photons that are both emitted and absorbed in the same cell are taken into account the correct formula for the counters S_{ij} becomes

$$
\begin{aligned}
S_{lu}(\nu) \; = \; & \frac{h\nu}{4\pi} B_{lu}\phi(\nu)\frac{s}{V} \\
& \{ \; (n^{\mathrm{T}}\frac{1 - e^{-\tau}}{\tau} + n_u A_{ul} V \phi(\nu)(1 - \frac{1 - e^{-\tau}}{\tau})) \\
& - \; (n^{\mathrm{R}}\frac{1 - e^{-t}}{t} + n_l A_{ul} V \frac{g_u}{g_l} e^{-\frac{h\nu}{kT_\mathrm{R}}}(1 - \frac{1 - e^{-t}}{t}))\}.
\end{aligned}
\tag{A13}
$$

If the reference field is not used the terms containing t are of course omitted.

References

Bernes C., 1979, A&A, 73, 67
Boisse P., 1990, A&A 228, 483
Choi M., Evans N.J., II, Gregersen E., Wang Y., 1995, ApJ 448, 742
de Jong T., Chu S.-I., Dalgarno A., 1975, ApJ 199, 69
Dickel H.R., Auer L.H., 1994, ApJ, 437, 222
Dickman R.L., Horvath M.A., Margulis M., 1990, ApJ 365, 568
Falgarone E., Phillips T.G., Walker C.K., 1991, ApJ 378, 186
Fischer O., Henning T., Yorke H.W., 1994, A&A 284, 187
Fischer O., Henning T., Yorke H.W., 1996, A&A 308, 863
Goldreich P., Kwan J., 1974, ApJ 189, 441
Gonzáles-Alfonso, E., Cernicharo, J., 1993, A&A 279, 506
Green S., Chapman S., 1978, ApJS, 37, 169
Hetem Jr. A., Lépine, J.R.D., 1993, A&A 270, 451
Houlahan P., Scalo J., 1992, ApJ 393, 172
Juvela, M., 1996, A&AS 118, 191
Knigge, C., Woods, J.A., Drew, E., 1995, MNRAS 273, 225
Lehtinen, K., Mattila, K., 1996, A&A 309, 570
Leung C.M., Liszt H.S., 1976, ApJ 208, 732
Liszt H.S., Leung C.M., 1977, ApJ 218, 396
Magnan C., 1970, J. Quant. Spectrosc. Radiat. Transfer. 10, 1
Marsaglia G., Zaman A., 1994, Computers in Physics, Vol 8, 1, 117
Mattila K., 1970, A&A 9, 53
Mazzali P.A., Lucy L.B., 1993, A&A 279, 447
Mazzali P.A., Danziger I.J., Turatto M., 1995,A&A 297, 509
Mundy L.G., Snell R.L., Evans N.J II, Goldsmith P.F., Bally J., 1986, ApJ 306, 670
Park Y.-S., Hong, S.S., 1995, A&A 300, 890
Park Y.-S., Hong S.S., Minh Y.C., 1996, A&A 312, 981
Press W.H., Teukolsky S.A., 1989, Computers in Physics, Vol 3, 6, 76
Rousselot P., Clairemidi J., Moreels G., 1994, A&A 286, 645
Rybicki G.B., Hummer D.G., 1991, A&A 245, 171
Sandford M.T., II, 1973, ApJ 183, 555
Spaans M., 1996, A&A 307, 271
Spaans M., van Langevelde H.J., 1992, MNRAS 258, 159
Turner B.E., Chan K., Green S., Lubowich D.A., 1992, ApJ 399, 114
van Blerkom D.J., 1971, ApJ 166, 235
Voshchinnikov N.V., Molster F.J., The P.S, 1996, A&A 312, 243
Whitney B.A., Hartmann L., 1992, ApJ 395, 529
Zhang Q., Wang Z.R., 1996, A&A 307, 166
Zhou S., Butner H.M., Evans N.J. II, et al., 1994, ApJ 428, 219
Zinchenko I., Forsström V., Lapinov A., Mattila K., 1994, A&A 288, 601